Supplemental Information for "Primary motor cortex reports efferent control of vibrissa motion on multiple time scales" by Daniel N. Hill, John C. Curtis, Jeffrey D. Moore and David Kleinfeld.

Figure S1. Representative map of the representation of vibrissa movement in vM1. Dots indicate a penetration site by a custom bipolar platinum-iridium stimulation electrode. Electrodes were lowered to a depth of 1.5 mm to excite neurons in L5 in the in the ketamine-anesthetized rat. The stimulation train was 1 s in duration, consisting of biphasic 200 μs pulses at 50 Hz with typical stimulation intensities of 10-100 μA. The site of recording electrode implantation used in recording experiments is indicated by an X. Grid size is 1 mm by 1 mm.

Figure S2. Synchronization of motion across columns and rows of vibrissae during whisking. (**A**) Motion parameters for a sample pair of simultaneously measured vibrissae for all periods where instantaneous peak-to-peak amplitude of the measured arc 1 vibrissa exceeded 15º. Phase, amplitude, and midpoint are computed as described Methods. (**B**) Correlation coefficients between all measured vibrissa pairs for the periods in A. The circular correlation coefficient is used to compare phase. (**C**) Similarity between motion parameters among sets of simultaneously measured vibrissae. Sets of position, amplitude, and midpoint traces were divided into non-overlapping 5s segments and principal components were computed separately for each segment (see Figure 1). Segments in which the mean peak-to-peak amplitude of the arc 1 vibrissa over the entire segment exceeded 15 degrees were included in the analysis. Each data point represents the proportion of variance explained by the first principal component in each segment as a function of the mean peak-to-peak amplitude of the measured arc 1 vibrissa over that entire segment. Independent motion of different vibrissae would result in a proportion of 1/N of the variance in the first mode, where N represents the number of vibrissae in the set. Inset: Correlation coefficients between measured pairs (as in B) as a function of inter-vibrissa Euclidean distance between the pair. Distance is measured in terms of the number of rows & arcs between the vibrissae in the pair. For example, C3 and D5 are 2 rows and 1 arc apart which corresponds to a distance of $\sqrt{(2^2 + 1^2)}$.

Figure S3. Histogram of spike widths of recorded units. Width was defined as the time difference between the negative and positive peaks of the mean waveform. The channel with waveform of larger amplitude was used for stereotrode data. Only units with negative initial peak were used (8 units excluded). Data from head-fixed, free-ranging, and nerve-cut experiments in vM1 cortex were merged. Dashed vertical line at 350 μs represents the cutoff used to separate narrow and wide waveforms.

Figure S4. Summary of the coding on fast and slow time scales based on EMG data for vM1 units recorded in free-ranging rats. (A) Scatter plot of the modulation depth for spike rate versus the magnitude of the EMG envelope (N = 69). Different colors distinguish increasing versus decreasing spike rate with an increase in EMG envelope, as noted. **(B)** Polar plot of the normalized modulation depth as a function of the preferred phase for the unit, ϕ_o; only points for significantly modulated units are plotted (N = 8). **(C)** Firing rates of all units during whisking and non-whisking behavior (N = 69).

Figure S5. Summary of the coding on fast and slow time scales based on EMG data for vS1 cortical units recorded from free-ranging or body-constrained rats. (A) Scatter plot of the modulation depth for spike rate versus the magnitude of the EMG envelope (N = 71). Different colors distinguish increasing versus decreasing spike rate with an increase in EMG envelope, as noted. **(B)** Polar plot of the normalized modulation depth as a function of the preferred phase for the unit, ϕ_o; only points for significantly modulated units are plotted (N = 33). **(C)** Firing rates of all units during whisking and non-whisking behavior (N=71).

Figure S6. Modulation profiles for three example units in vM1 cortex after transection of the sensory nerve. (A) Diagram of the IoN branch of the trigeminal nerve, along with the mean LFP response in vS1 cortex to 50 puffs to the vibrissa shown before and after bilateral nerve transection**. (B)** Modulation profiles for example units, with the respective stereotrode waveforms and spike train autocorrelations shown at top. The columns are profiles of units that show different relative modulation by slow and fast whisking parameters. Each plot is calculated by dividing the distribution of the respective parameter at spike time by the distribution of that parameter over the entire behavioral session. Green lines are fits from BARS smoothing

algorithm along with 95 % confidence band. The symbol ϕ_o labels the peak of the tuning curve, or the preferred phase for spiking within the whisk cycle.

Figure S7. Estimated accuracy of coding in vM1 cortex as a function of population size. (A) Simulation results for units from normal animals. Simulations of neuronal populations were either based on the entire measured data set (black line) or only on the unit with the highest recorded modulation depth (gray line). Errors were drawn from 1000 simulations of each value and weighted by their prior distributions. *Top row.* Mean error for amplitude estimation assuming an integration time of T = 0.25 s. *Middle row.* Mean error for midpoint estimation assuming an integration time of T = 0.25 s. *Bottom row.* Mean error for phase estimation. (**B**) Simulation results for units from animals with transected IoNs. Layout as in panel A.

Figure S8. Schematic of simulation design used to estimate population coding of midpoint and amplitude. The case of amplitude, θ_{amp}, is used for illustration, but the analysis of midpoint is similar. At left are the response profiles of firing rate as a function of amplitude for the recorded single unit that corresponds to the simulated unit. Next column to the right shows the probability of a simulated unit firing a particular number of spikes given an integration time (τ = 1 s) and value of the amplitude ($\theta_{amp} = 55^o$). The spike counts are assumed to be independent between units and drawn from a Poisson distribution. At bottom of this column is the a priori distribution of amplitude, $p(\theta_{amp})$, calculated from the average value of θ_{amp} at each percentile from all behavioral sessions. The third column shows example posterior distributions for amplitude conditioned on simulated spike counts. One trace is darkened to illustrate the MAP estimate of amplitude, $\hat{q}_{amp;m}$, which is at the trace's peak. The fourth column shows the distribution of $\hat{q}_{amp;m}$ from 1000 simulations when $\theta_{amp} = 27^o$. Then in the final column is the error of the estimator, $\delta\theta_{amp;m}$, for all values of θ_{amp}.

Figure S9. Schematic of simulation design used to estimate population coding of phase. At left are 2D histograms that characterize the error in phase prediction for the transfer function of a single unit. The ordinate represents the measured phase, ϕ, and the abscissa represents the error in phase prediction by the k^{th} simulated unit, $\Delta f_k = x_k - f$. The color bar is normalized

to the maximum probability as only relative probability is relevant in the model. Next column to the right shows the probability of the estimate of phase by single units, given a particular measured phase, $\phi = \pi/4$, At bottom is the a priori distribution of phase, $p(\phi)$, calculated from all behavioral sessions. The third column shows example posterior distributions for phase given sampling of all simulated units. One trace is darkened to illustrate the maximum *a priori* estimate, $\hat{f}$, of phase. The fourth column shows the distribution of $\hat{f}$ from 1000 simulations when $\phi = \pi/4$. Then in the final column is the error of the estimator, df, for all values of ϕ.

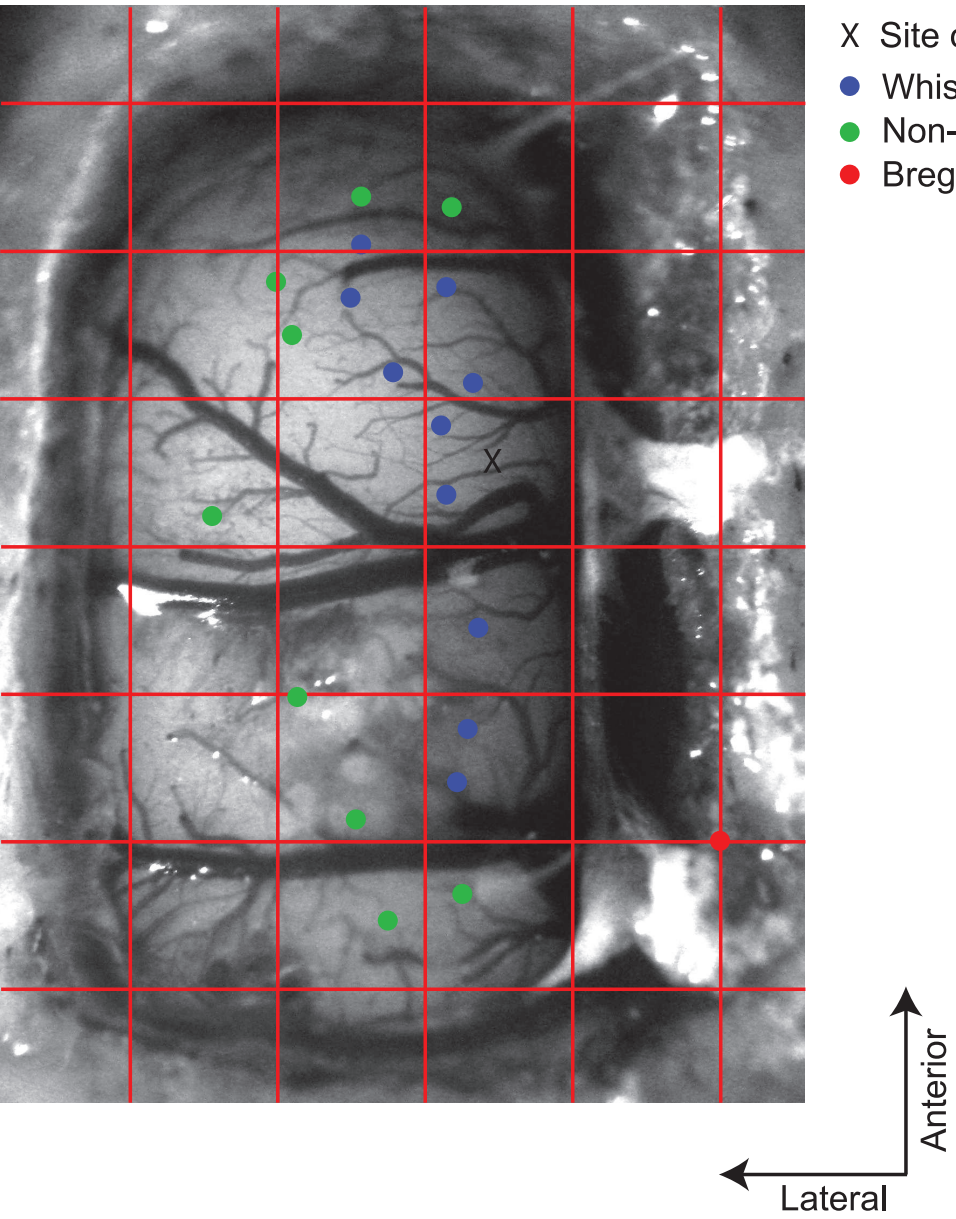

Supplementary Figure S1 - Hill, Curtis, Moore & Kleinfeld

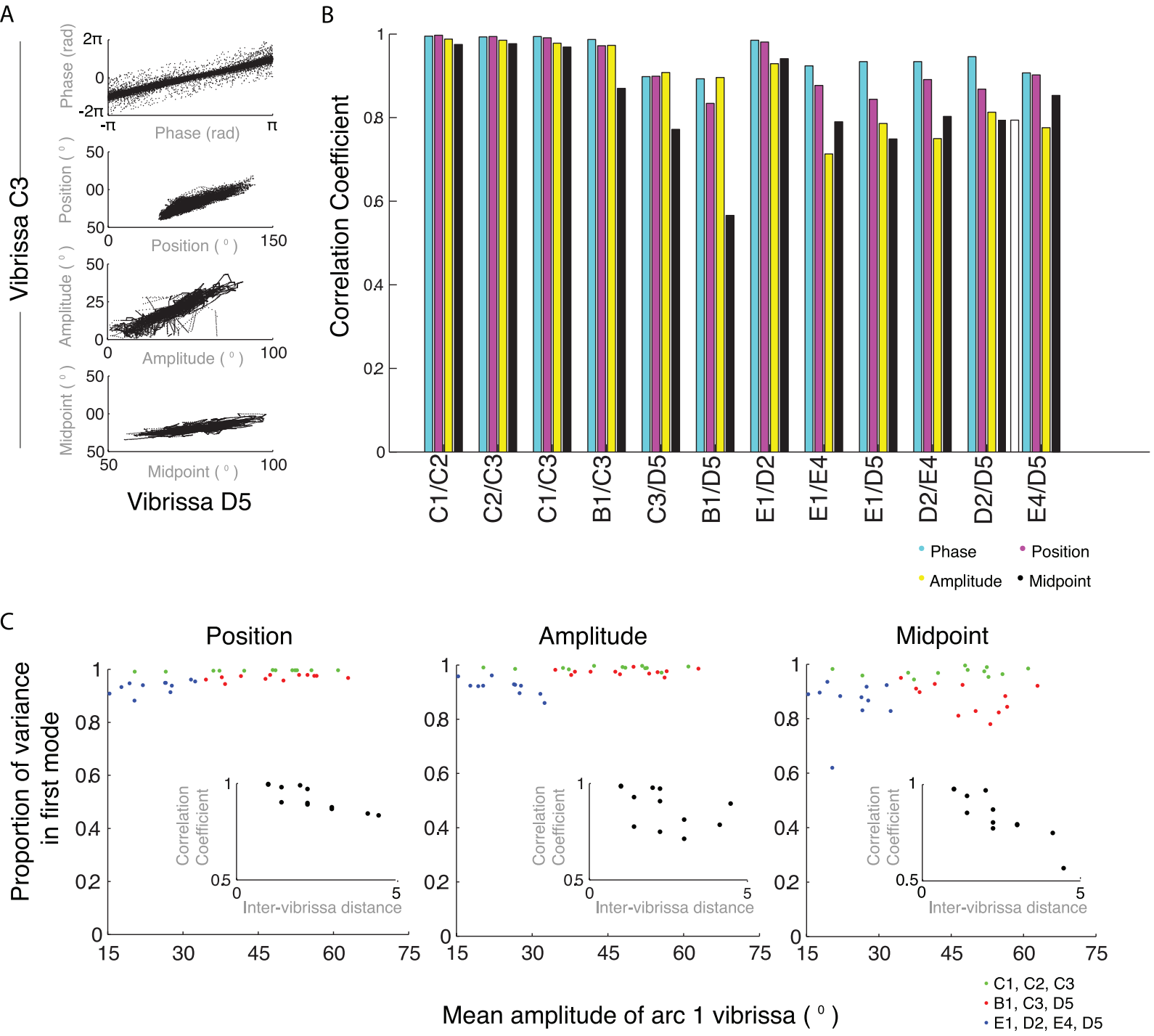

Supplementary Figure S2 - Hill, Curtis, Moore & Kleinfeld

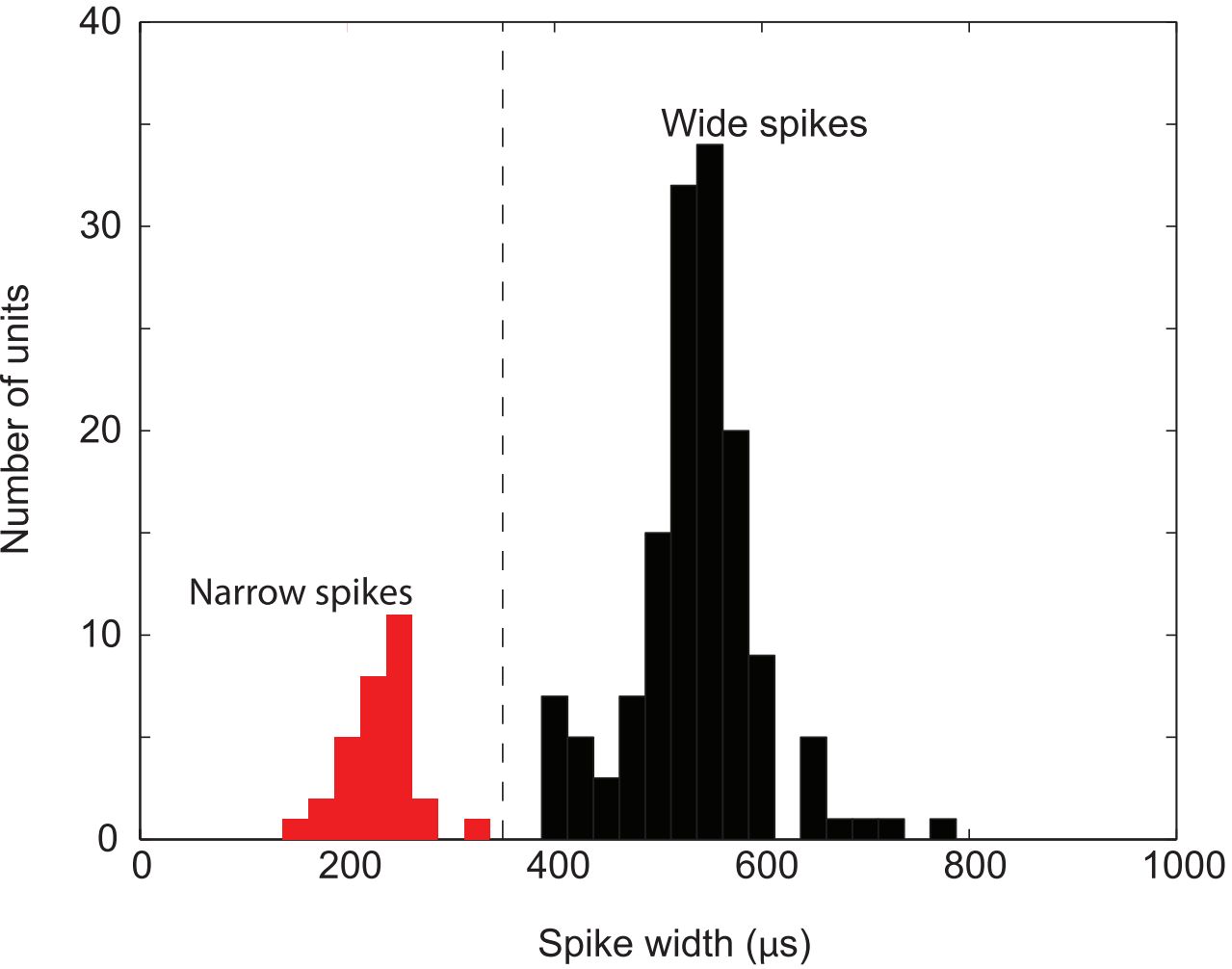

Supplementary Figure S3 - Hill, Curtis, Moore & Kleinfeld

A

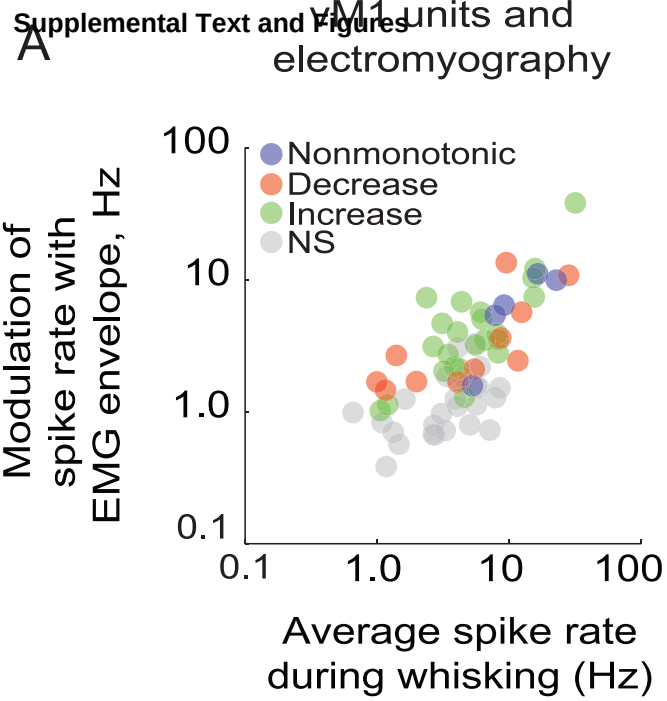

B

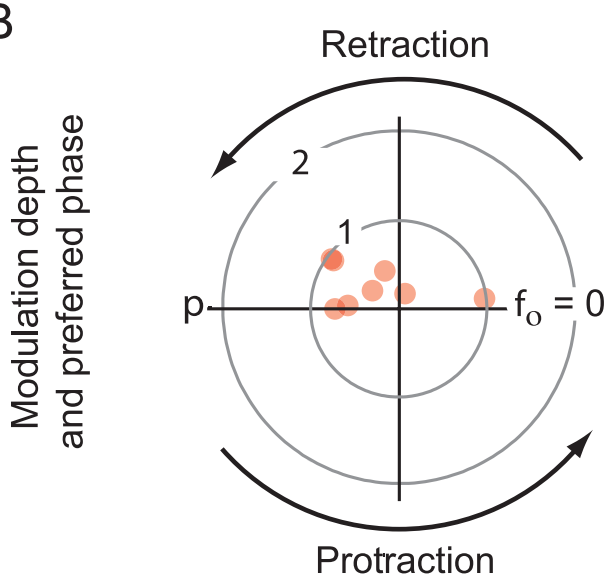

C

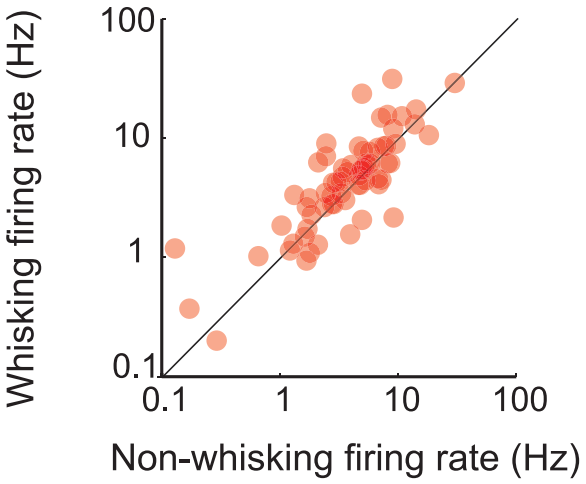

Supplementary Figure S4 - Hill, Curtis, Moore & Kleinfeld

A

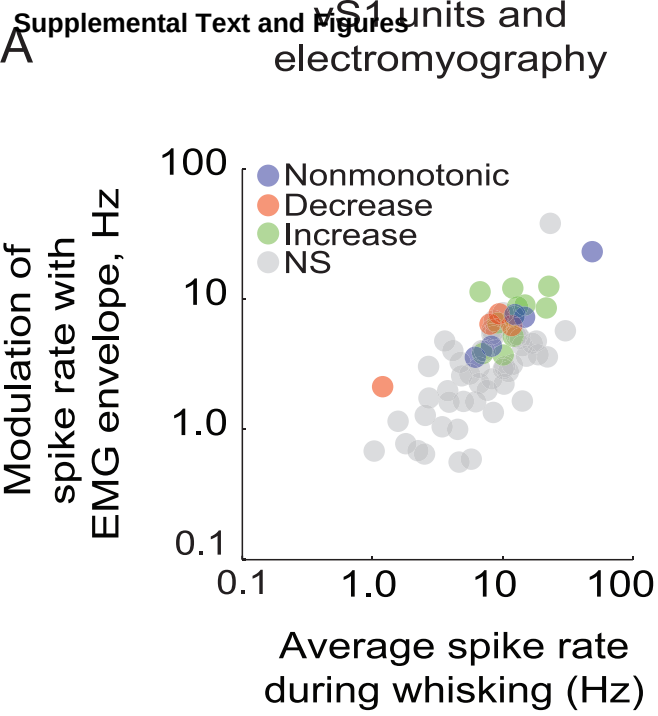

B

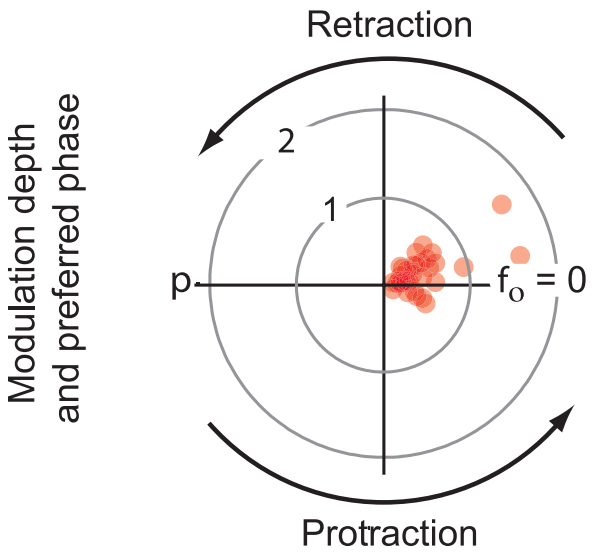

C

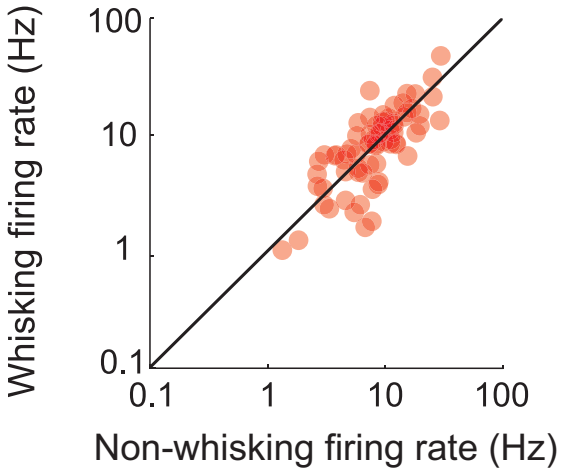

Supplementary Figure S5 - Hill, Curtis, Moore & Kleinfeld

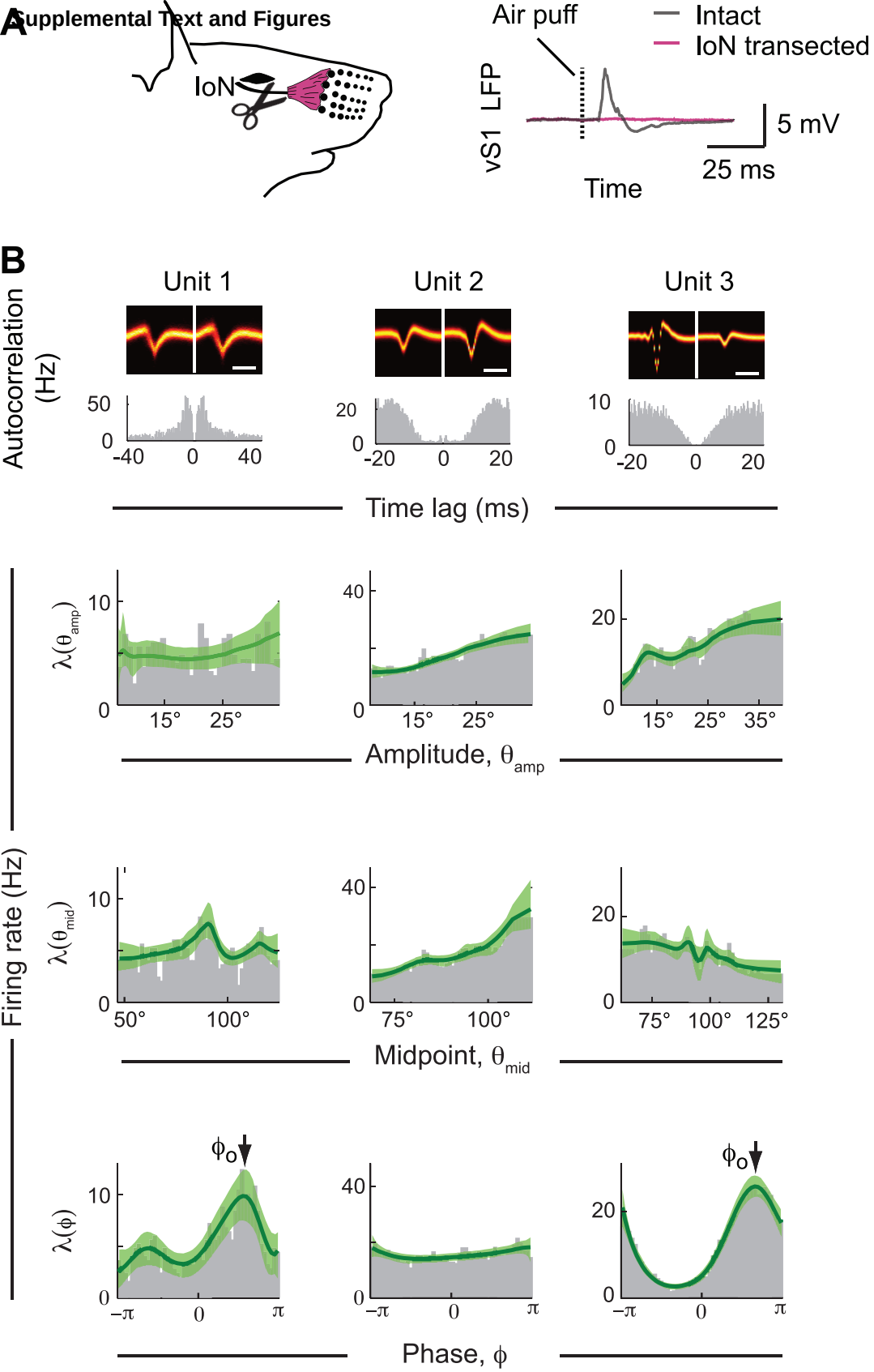

Supplemental Figure S6 - Hill, Curtis, Moore & Kleinfeld

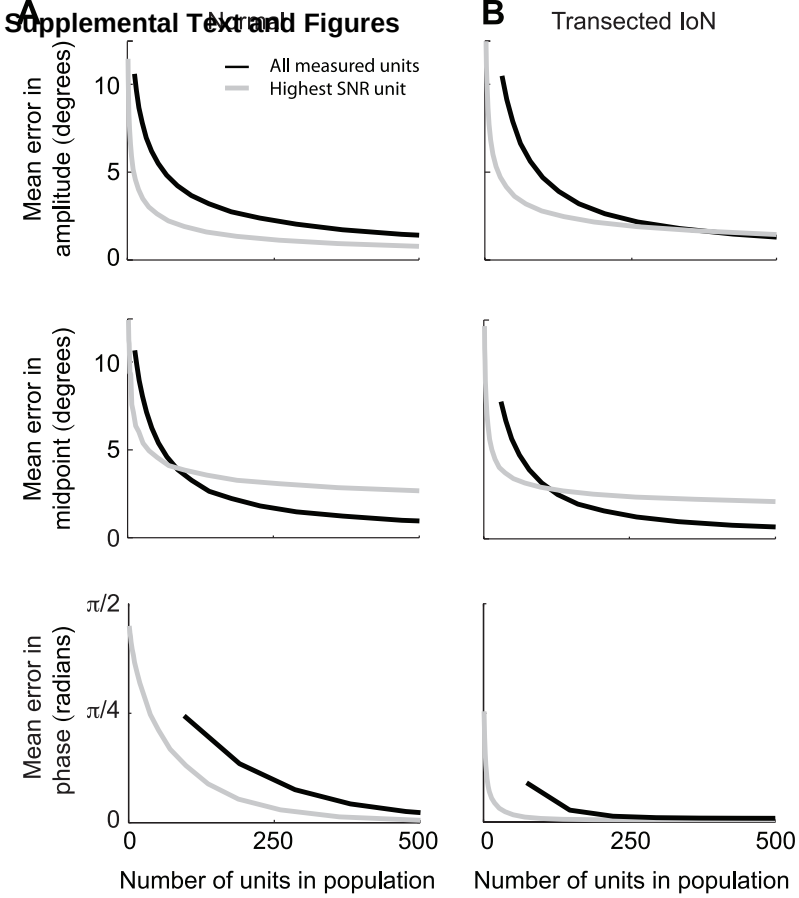

Supplemental Figure S7 - Hill, Curtis, Moore & Kleinfeld

Figure 8 - Hill, Curtis, Kleinfeld

Supplemental Text and Figures

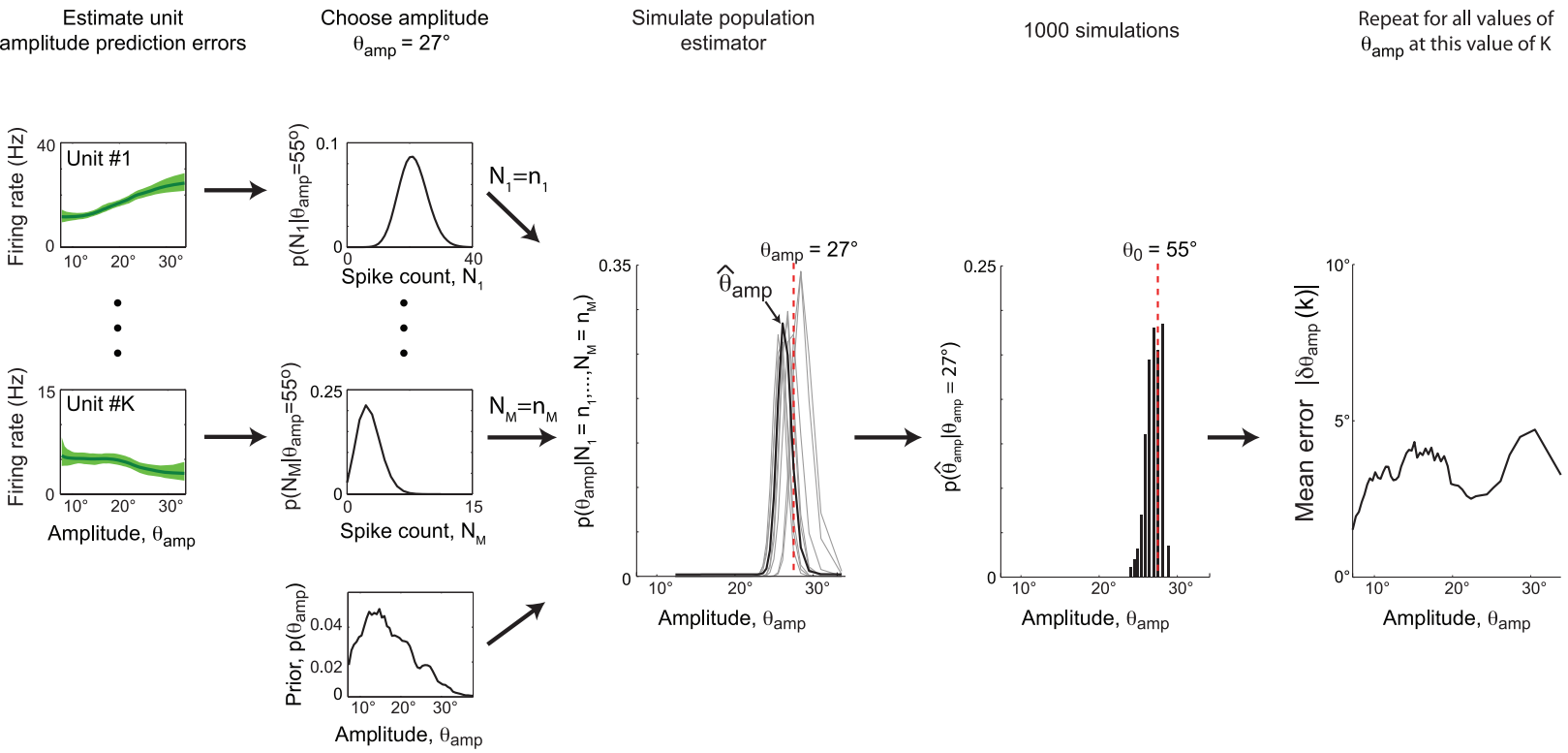

Supplemental Figure S8 - Hill, Curtis, Moore & Kleinfeld

Supplemental Text and Figures

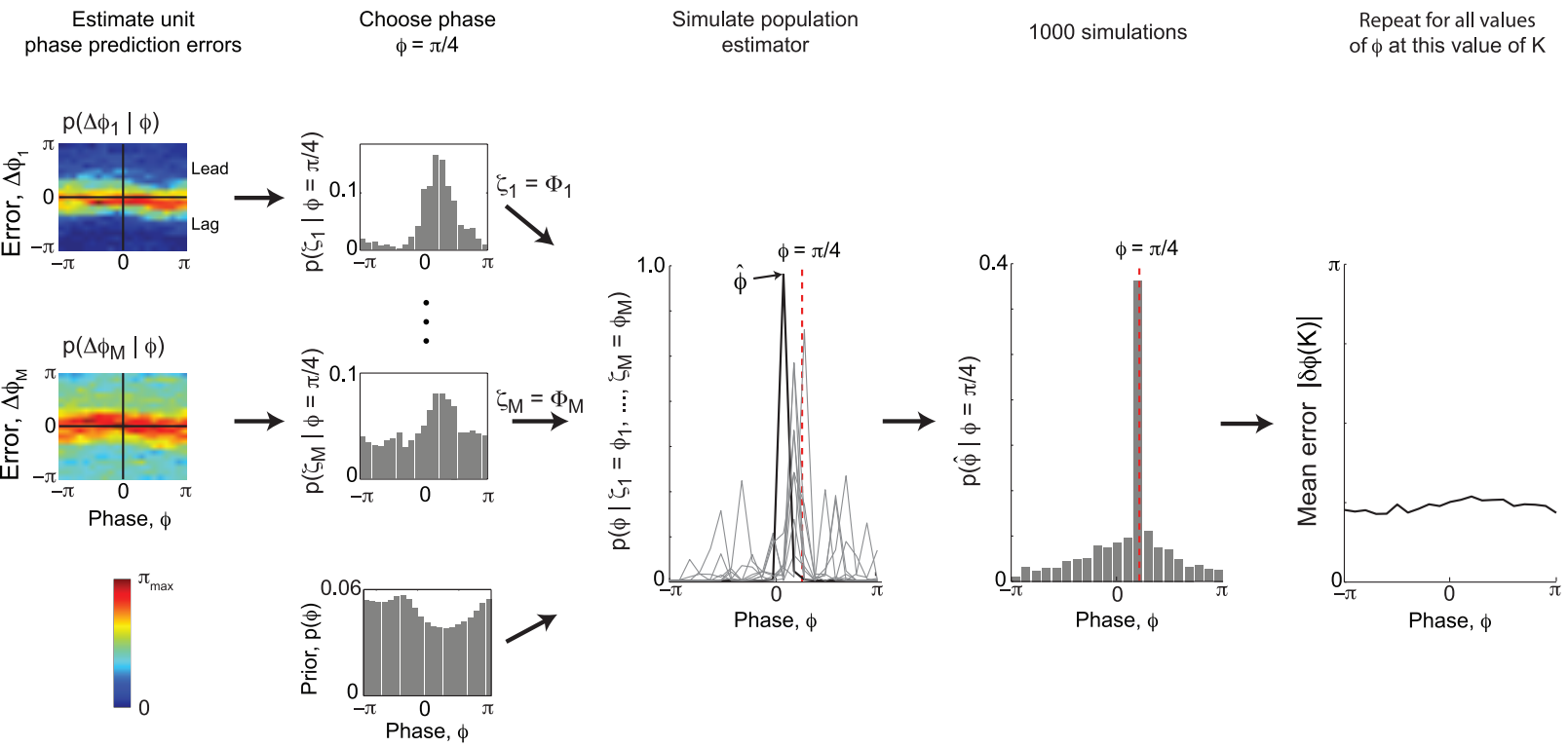

Supplemental Figure S9 - Hill, Curtis, Moore & Kleinfeld